NUMERICAL SIMULATION AND VISUALIZATION MODELS OF STRESS WAVE PROPAGATION GRAPHITE/EPOXY COMPOSITES

R.D. Kriz

Institute for Materials Science and Engineering
National Institute of Standards and Technology
325 Broadway
Boulder, CO 80303

J.M. Gary

Center for Computing and Applied Mathematics
National Institute of Standards and Technology
325 Broadway
Boulder, CO 80303

INTRODUCTION

Within the last ten years there has been a renewed interest in simulation of stress wave propagation because of the availability of fast supercomputers with large memory capabilities [1,2,3]. Only recently have a few investigators [4,5] applied these simulations to problems where elastic anisotropy was included as a major factor. The massive output of results from these simulations, together with the added complexity of coupled phenomena that uniquely exist for a given anisotropy, defies intuition. To grasp the significance of these simulations requires scientific visualization [6] of these complex physical phenomena. Such visualizations often require a movie format to better understand the physics of particular problems [7]. In this study we simulated the experimental measurement of a shift in the quasi-transverse bulk wave propagation in an off-axis unidirectional graphite/epoxy composite in plane strain [8]. The purpose of the simulation was to aid the nondestructive evaluation engineer in designing an acoustic array to improve the measurement of the shift in the QT wave propagation direction [9]. Previously a finite element model [5] was used to simulate this measurement. In this study we demonstrate the advantages of using a finite difference model to simulate this experiment and, with special visual aids, observe the physics.

Finite Difference Method

We modified the finite difference method of Bayliss, et al. [10] to include elastic anisotropy with nonreflecting (absorbing) or reflecting boundary conditions from either a rigid or stress-free planar boundary.

Review of Progress in Quantitative Nondestructive Evaluation, Vol. 9
Edited by D.O. Thompson and D.E. Chimenti
Plenum Press, New York, 1990

The equations of motion are written below as a first order hyperbolic system of five partial differential equations where the unknown velocities ($\dot{u}$,$\dot{v}$) and stresses (σ_{xx}, σ_{yy}, σ_{xy}) are differentiated only once with respect to space and time,

$$\rho \frac{\partial \dot{u}}{\partial t} = \frac{\partial \sigma_{xx}}{\partial x} + \frac{\partial \sigma_{xy}}{\partial y}, \qquad \rho \frac{\partial \dot{v}}{\partial t} = \frac{\partial \sigma_{xy}}{\partial x} + \frac{\partial \sigma_{yy}}{\partial y},$$

$$\frac{\partial \sigma_{xy}}{\partial t} = C_{11} \frac{\partial \dot{u}}{\partial x} + C_{12} \frac{\partial \dot{v}}{\partial y} + C_{16} \left(\frac{\partial \dot{u}}{\partial y} + \frac{\partial \dot{v}}{\partial x} \right), \tag{1}$$

$$\frac{\partial \sigma_{xy}}{\partial t} = C_{16} \frac{\partial \dot{u}}{\partial x} + C_{26} \frac{\partial \dot{v}}{\partial y} + C_{66} \left(\frac{\partial \dot{u}}{\partial y} + \frac{\partial \dot{v}}{\partial x} \right),$$

$$\frac{\partial \sigma_{yy}}{\partial t} = C_{12} \frac{\partial \dot{u}}{\partial x} + C_{22} \frac{\partial \dot{v}}{\partial y} + C_{26} \left(\frac{\partial \dot{u}}{\partial y} + \frac{\partial \dot{v}}{\partial x} \right),$$

where C_{ij}, $i = 1,2,6$ are contracted Vogt notation of the general stiffness tensor C_{ijkl}. The advantage of this formulation is the absence of mixed second order derivatives ($\partial^2/\partial x \partial y$) with only first order derivatives so that the method of characteristics can be used to construct the necessary boundary conditions. The numerical method described in detail in reference 10 is accurate to fourth order in space and accurate to second order in time, and uses a splitting method which is well suited to vector computers. Here we will expand only on the approximation of the boundary conditions.

Boundary Conditions

For calculating the boundary conditions, we rewrite the equations of motion, (1), in matrix/vector form,

$$\frac{\partial w}{\partial t} + A \frac{\partial w}{\partial x} + B \frac{\partial w}{\partial y} = 0 \tag{2}$$

where $w^T = (\dot{u},\dot{v}, \sigma_{xx}, \sigma_{xy}, \sigma_{yy})$ and the matrices A and B are constant. The domain is a rectangle in (x,y) space. Consider the boundary condition along the left side, $x = 0$; see Figure 1. Let P be the matrix of eigenvectors of the A matrix such that

$$P^{-1} AP = D, \tag{3}$$

where D is the diagonal matrix of eigenvalues. The equations of motion, (2), can be written in terms of a transformed set of variables (characteristic variables), $v = P^{-1}w$, by the following:

$$P^{-1} \frac{\partial w}{\partial t} + P^{-1}APP^{-1} \frac{\partial w}{\partial x} + P^{-1} \frac{\partial w}{\partial y} = 0, \tag{4}$$

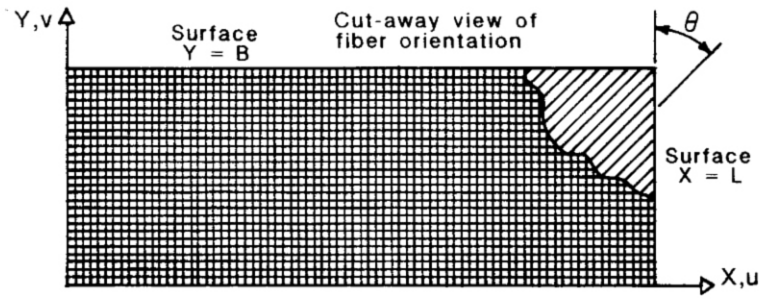

Figure 1. Definition of finite difference mesh.

or in terms of v,

$$\frac{\partial v}{\partial t} + D\frac{\partial v}{\partial x} + B\frac{\partial v}{\partial y} = 0. \tag{5}$$

The variables v_i correspond to the eignevalues of D. Positive eigen-values are "inflow" characteristic variables and negative eigenvalues define "outflow" characteristic variables. Along these boundaries Bayliss [10] extrapolates the solution to the two mesh points adjacent to the computational mesh using the relations:

$$\begin{aligned} f_{n+1} &= 4f_n - 6f_{n-1} + 4f_{n-2} - f_{n-3}, \\ f_{n+2} &= 4f_{n+1} - 6f_n + 4f_{n-1} - f_{n-2}, \end{aligned} \tag{6}$$

so that the fourth order difference scheme can be computed over the entire computational mesh including the boundary points.

Once the difference scheme has advanced the solution to the next time step over the entire computational mesh, then the boundary values are corrected using the characteristic linear combinations acquired from the diagonalization of the equations of motion in the direction normal to the boundary. If

$$v_i = \sum_{j=1}^{5} P_{ij}^{-1} w_j \tag{7}$$

is an "outflow" characteristic, then its value is calculated from the finite difference approximation, (6). Denote the boundary values computed at the new time step by $\tilde{w}^{n+1}$. The final boundary values, which we denote by w^{n+1}, should give the following relation:

$$\sum_{j=1}^{5} P_{ij}^{-1} w_j^{n+1} = \sum_{j=1}^{5} P_{ij}^{-1} \tilde{w}_j^{n+1}, \tag{8}$$

for the outflow linear combination; that is, for each value of i corresponding to an outflow characteristic.

At each boundary there are three outflow variables, thus three equations of the form of (8). The inflow conditions give two additional equations for the values of w^{n+1} at the boundary. In summary, there are five equations for the five unknown w^{n+1} to give the boundary values.

Solution and Mesh Definition

The solution of equations, (1) with appropriate boundary conditions proceeded as outlined above and in reference [10]. Nonreflecting boundaries were assigned at x=0, x=L, and y=B. At the boundary y=0 a stress wave was launched by prescribing velocities ($\dot{u}$,$\dot{v}$) that would simulate the response of an idealized longitudinal transducer vibrating sinusoidally. The transducer displacement field was idealized as a spatial Gaussian distribution over 101 mesh points along y=0 with a 25 mesh point approximation for one wavelength. The wave period was divided into 160 time steps. The elastic stiffnesses, C_{ij}, were calculated for fiber orientations from $\theta = 0^0$ to $\theta = 90^0$ in increments of 10^0. These stiffnesses were identical to those reported in Reference 5.

For an off-axis orientation, $0^0 < \theta < 90^0$, the conditions prescribed above resulted in the simultaneous generation of quasilongitudinal (QL) and quasitransverse (QT) waves that propagated along deviated paths. This particular problem was chosen to verify the accuracy of the simulation to reproduce the deviated propagation directions predicted by plane wave theory. In addition, this problem was also chosen to verify the measurement of the deviated QT wave as outlined in reference [8].

Because of the deviated propagation directions of the QL and QT waves, the position of the source along y=0 and the mesh dimensions were sized to avoid propagation of waves into corners. For all cases of fiber orientations a mesh size of 451 points along the x-coordinate and 126 points along the y-coordinate resulted in stable solutions where QL and QT waves remained sufficiently far from the mesh corners. To verify the accuracy of these solutions, larger grids (1001 x 161) with 40 points per wavelength and 240 time steps per period yielded results with only small improvements. Total solution time was established when the slower moving QT wave arrived at the far boundary y=B. The standard mesh (451 x 126) required 20 minutes of computation time and 200000 single precision words of memory compared to 2.2 hours and 3.2 million words of memory for the finite element solution in reference 5.

EXACT SOLUTION

An exact theoretical solution is necessary to verify the accuracy of the simulation. The exact solutions for plane stress and plane strain are given in reference 5, but here we have considered only plane strain and list only the most relevant equations.

Christoffel's Solution

Stress-wave deformation fields in anisotropic media can be approximated by plane wave solutions to the elastic-wave equation. This simplification leads to Christoffel equation [11]:

$$(C_{ijk\ell}\,\nu_j\nu_k - \rho v^2\delta_{i\ell})\,p_\ell = 0 \qquad (9)$$

where $C_{ijk\ell}$ is the elastic-stiffness tensor, ν_j the wave vector, ρ the mass density, v the wave velocity (eigenvalue), $\delta_{i\ell}$ the Kronecker delta,

and p_ℓ the direction of particle vibration (eigenvector). Solutions in the principal material planes are given in [12], where it is shown that the particle motion is confined to the principal material plane and decouples from the out-of-plane vibrations. Hence the plane strain solutions and bulk wave solutions of Equation (9) are identical when confined to principal material planes. For plane stress, the solution of (9) is modified by reducing the stiffness, see [5].

Flux Deviation

Musgrave [11] demonstrated graphically how the propagation direction can deviate from the wave vector. This direction is called the energy flux deviation vector,

$$E_j = -C_{ijk\ell}\, u_{k,\ell}\, \dot{u}_i, \tag{10}$$

where u_i is the displacement vector for plane wave. The velocity of propagation in the direction of E_j is called the group velocity. For anisotropic materials E_j deviates from ν_i by an angle, $\Delta = \cos^{-1}\nu_i E_i$.

RESULTS AND DISCUSSION

The finite difference solution of (1) for the region described in Figure 1 was obtained for fiber orientations from θ=0 to θ=90^0 in increments of 10^0. Results are plotted in Figure 2 and compared with the finite element solution from reference 9 and the exact solution of (10). Improved results from the finite difference solution are observed over the range $0^0 < \theta < 70^0$. This improvement was accomplished not only by increasing the number of time steps per period and increasing the number of mesh points per wavelength, but mostly by preferentially launching either the QT or QL wave by prescribing the correct ratio of longitudinal to transverse particle motion predicted by the eigenvector, p_ℓ, solution to the Christoffel's equation (9). This approach is shown more clearly with visual aids in Figures 3 and 4.

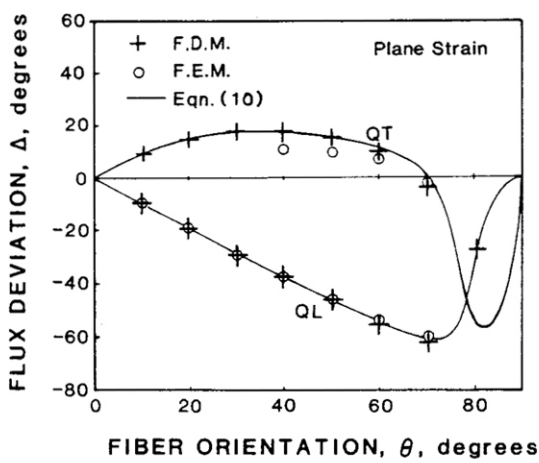

Figure 2. Comparison of finite difference model, (F.D.M.), finite element model, (F.E.M.) and exact solution in plane strain.

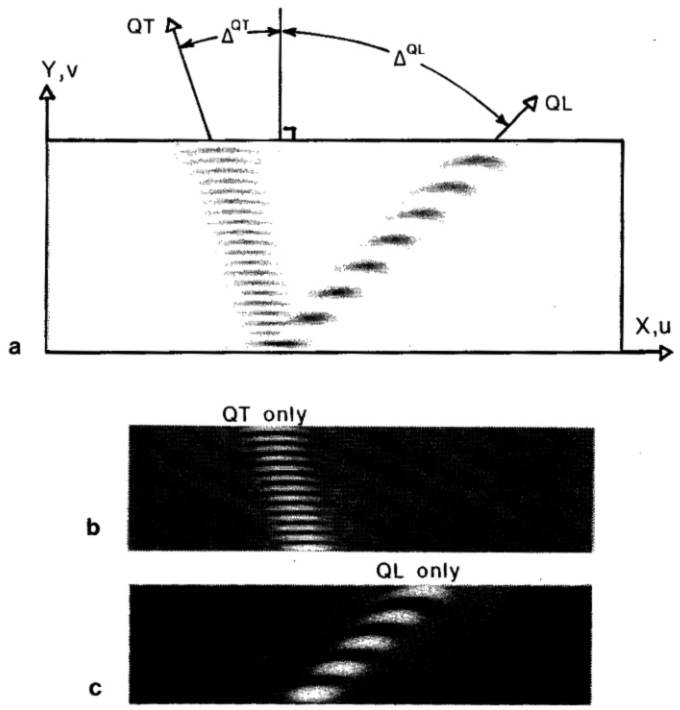

Figure 3. a) Gray scale representation of u displacements for the QL and QT waves propagating in unidirectional graphite/epoxy composite in plane strain at $\theta = 50^0$; b) preferential launching of the QT wave; c) preferential launching of the QL wave.

In Figure 3a we show a gray scale representation of the u displacements generated by a simulated longitudinal transducer in a unidirectional graphite/epoxy composite whose fiber axis is oriented at $\theta=50^0$ from the y-axis. At this orientation, theory predicts equal u and v displacements for both QT and QL waves and both waves are well separated. Because both waves have a v component of displacement along the y-axis, the longitudinal transducer will generate both waves. If, however, the ratio of longitudinal to transverse wave motion generated along the boundary, y=0, is equivalent to the eigenvector, P_ℓ, corresponding to the QT eigenvalue, then only the QT wave will be generated (see Figure 3b). Similarly only the QL wave may be generated by its unique eigenvector. Obviously, this technique can be used to separate the QT and QL waves, at the small angles of θ, where they would otherwise interfere.

In Figures 4a and 4b we show how the isolation of the QT wave can also be used to improve the measurement proposed in reference 8. The slower moving QT wave (lower right) and the faster moving QL wave (upper left), shown in Figure 4a as a displaced out-of-plane shaded surface, were generated simultaneously from the same unipolar pulse. Here the objective was to simulate and measure the propagation direction of the QT wave by using a linear array of acoustic transducers on the reflecting

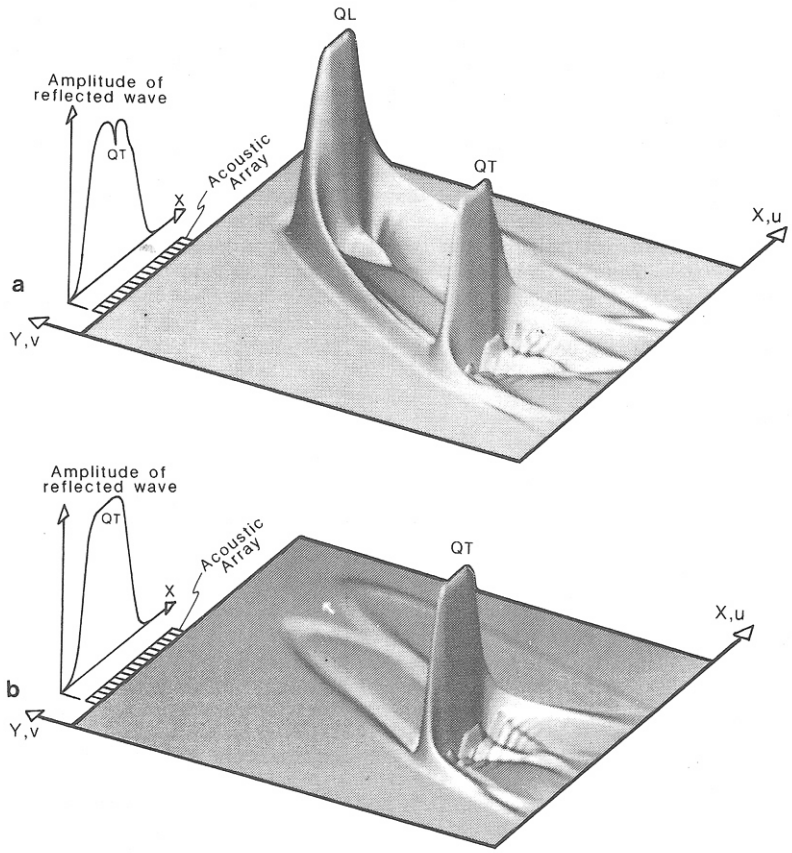

Figure 4. a) In-plane v-displacements for QL and QT waves visualized as shaded-out-of-plane surfaces where the wave shape of the QT wave is measured by the acoustic array with double peaks; b) preferential launching of the QT wave where the shape of the QT wave measured by the same acoustic array shows no double peaks and the white arrow points to where the QL wave has been eliminated.

boundary. Because the angle of propagation, and not simply the QT wave arrival time is measured, it is necessary to measure the wave shape. This measurement gave peculiar multiple peaks whose physical origin was unexplained. A simulation and visualization in a movie format [7] clearly showed that the physical origin of these multiple peaks was the generation of "wakes" from the faster moving QL wave. Preferential launching of the QT wave (see Figure 4b), with its unique eigenvector, eliminated the QL wave and its wakes; this suggested that an improved measurement of the direction of propagation of the QT wave was physically possible if a transducer could be designed to reproduce the eigenvector ratio of longitudinal to transverse displacements. Possibly a specially cut quartz transducer would satisfy these requirements.

CONCLUSIONS

A simulation that used the finite difference solution was less stable than the finite element solution near boundaries but was much more accurate, required ten times less memory, and was 66 times faster. Both numerical methods were simple programs that did not require extensive experience to implement. The visualization of the simulation results provided the necessary insight to understand the physical origin of the experimental anomalies. Visualization of the simulation results, together with theoretical predictions, suggest a solution that would remove the anomalies by preferentially generating the QT wave with its unique eigenvector. Together with experiment and theory, we demonstrated how numerical simulation and visualization was used to better understand and improve measurements by an existing NDE method.

ACKNOWLEDGEMENTS

The authors would like to express their gratitude to Precision Visuals Inc. for providing the visual aid software and Mike Maish, Dave Lovering, and Sean Coleman of NIST for their network and system administration support.

REFERENCES

1. R. Ludwig and W. Lord, Materials Evaluation 46, 108 (1988).
2. Z. You, W. Lord, and R. Ludwig, in Review of Progress in Quantitative NDE, edited by D. O. Thompson and D. E. Chimenti (Plenum Press, New York, 1988), Vol. 7A, pp. 23-30.
3. N. Saffari and L. J. Bond, J. Nondestructive Evaluation 6, 1 (1987).
4. J. A. G. Temple, J. Phys. D: Apl. Phys. 21, 859 (1988).
5. R. D. Kriz and P. R. Heyliger, in Review of Progress in Quantitative NDE, edited by D. O. Thompson and D. E. Chimenti (Plenum Press, New York, 1989), Vol. 8A, pp. 141-148.
6. B. H. McCormick, T. A. Defanti, and M. D. Brown, "Visualization in Scientific Computing," National Science Foundation Report prepared under Grant ASC-8712231, July 1987.
7. R. D. Kriz, "Movies Reveal Secrets of Materials", NIST Research Reports, NIST-STP765, NIST, Gaithersburg, MD 20899.
8. R. D. Krix, "Systems for Monitoring Changes in Elastic Stiffness in Composite Materials," United States patent no. 4,499,770 (Feb. 19, 1985).
9. D. W. Fitting, R. D. Kriz, and A. V. Clark, Jr., in Review of Progress in Quantitative NDE, edited by D. O. Thompson and D. E. Chimenti (Plenum Press, New York, 1989), Vol. 8B, pp. 1497-1504.
10. A. Bayliss, K. E. Jordan, B. J. LeMesurier, and E. Turkel, Bulletin of the Seismological Society of America, Vol. 76, No. 4, pp. 1115-1132, August 1986.
11. M. J. P. Musgrave, Crystal Acoustics (Holden-Day, San Francisco, 1970).
12. R. D. Kriz and H. M. Ledbetter, in Recent Advances in Composites in the United States and Japan, edited by J. R. Vinson and M. Taya (American Society for Testing and Materials, Philadelphia, 198), pp. 661-675.